

Non-Hermitian Stark Many-Body Localization

Han-Ze Li¹, Xue-Jia Yu², and Jian-Xin Zhong^{1,*}

¹ School of Physics and Optoelectronics, Xiangtan University, Xiangtan 411105, China

² International Center for Quantum Materials, School of Physics, Peking University, Beijing 100871, China

(Dated: May 17, 2023)

By employing the method of Exact Diagonalization (ED), we examine a one-dimensional non-Hermitian hard-core boson chain imbued with a Stark gradient potential and a tail curvature. In this non-Hermitian system, we witness the occurrence of Many-Body Localization (MBL) phase transitions and real-complex transitions. Further analysis of the entanglement entropy's dynamical behavior reveals its similarity with that of disordered-driven non-Hermitian MBL systems, even though the dynamical response of the real part of the eigenenergy is less pronounced. We also map out the phase diagrams for non-Hermitian strength versus Stark gradient potential strength, and interaction strength versus Stark gradient potential strength, discovering that an intermediate phase exists in the non-Hermitian Stark MBL system as well. Overall, our findings provide a new platform for studying disordered-free non-Hermitian MBL, holding direct relevance to experimental research in ultracold atomic systems.

I. INTRODUCTION

Non-Hermitian quantum systems have sparked a surge of research interest over the past two decades [1–32], owing to their unique capabilities in hosting an array of remarkable physical phenomena not present in Hermitian quantum systems, such as real-complex transitions of eigenenergies, the topology of exceptional points, and non-Hermitian skin effects, etc [33–41]. Among these, the transition from real to complex eigenenergies and the metal-insulator phase transition are typically associated with the parity-time (\mathcal{PT}) symmetric broken in non-Hermitian quantum system [42]. However, interestingly, recent findings reveal that in a class of random or quasiperiodic non-Hermitian quantum many-body systems lacking \mathcal{PT} symmetry but possessing time-reversal symmetry (TRS), the variation in disorder strength not only induces MBL phase transitions also drives through the real-complex transition [43–46]. Although random and quasiperiodic systems do not belong to the same universality class [47, 48], disorder strength serves as the primary driving factor for both system types. But, for many-body quantum systems, disorder is not a necessary condition to induce the MBL phase transition [49, 50].

It should be emphasized that a class of disorder-free systems can also host MBL phase transitions and exhibit properties similar to those of disorder-induced MBL during the MBL phase, such as non-thermal eigenstates and the manifestation of non-equilibrium dynamics characteristics [51–53]. It represents the generalization of Wannier-Stark localization [54] from single-particle to many-body scenarios, known as Stark Many-body Localization (SMBL) [51–53]. In SMBL, the driving force of the MBL phase transition is determined by the strength of the external field [53]. Compared to disorder-driven MBL, SMBL systems exhibit simpler and cleaner features [52], particularly in experimental settings such as

ion trap platforms [51] and superconducting circuit platforms. In terms of numerical computations, SMBL systems also demand less computational resources than disordered systems [55].

For non-Hermitian quantum many-body systems, on the one hand, localization suppresses the imaginary part of the eigenenergies [43], leading to the real-complex transition. The real-complex transition is a phenomenon that occurs in non-Hermitian interacting systems with asymmetric hopping, which respects time-reversal symmetry. It represents a transition point where almost all eigenenergies become real, and energy absorption or emission disappears despite non-Hermiticity, indicating that quantum states attain dynamic stability. The real-complex transition exerts a significant influence on the dynamic stability of non-Hermitian interacting systems [43]. On the other hand, recent results indicate that in non-Hermitian quantum systems, the emergence of a metal-insulator transition is accompanied by a change in topological invariant, leading to a topological phase transition [42]. In the case of interacting systems, variations in the parameter controlling the MBL phase transition result in alterations to the winding number of the complex spectra, revealing a topological phase transition as the potential field amplitude increases. The origin of the topological phase transition in this model exhibits significant differences from that in single-particle systems [44].

Consequently, examining systems that can exhibit MBL phase transitions, real-complex transitions, and topological phase transitions, as well as the interrelationships between these transitions, has become increasingly significant in non-Hermitian quantum many-body systems. However, current research has primarily focused on disordered non-Hermitian quantum many-body systems, with limited attention given to non-Hermitian SMBL systems.

In the remainder of the paper, we investigate the MBL phase transitions and real-complex transition in non-Hermitian many-body system with Stark gradient

* jxzhong@xtu.edu.cn

potentials. Through numerical calculations on a one-dimensional hard-core bosonic model with periodicity, we demonstrate the existence of MBL phase transitions, real-complex transitions in this model, and discuss the interrelationships between these two types of transitions. Next, we turned our attention to the dynamical statistics of the system. Intriguingly, the dynamical profile of the entanglement entropy mirrored that of a system subjected to disorder. Yet, the dynamical response of the real part of the energy didn't exhibit such disorder-like behavior. Ultimately, we depicted phase diagrams with the Stark gradient potential strength γ and the non-Hermitian strength g , and also with γ and the interaction strength U . Within these phase diagrams, we identified regions bearing a striking resemblance to those found in phase diagrams of non-Hermitian models subjected to disorder [56]. Our exploration furnishes a novel platform for delving into non-Hermitian many-body localization phase transitions, with easy applicability for experimental validation in systems such as cold atoms.

II. MODEL AND METHODS

We consider a one-dimensional hard-core boson model with a Stark gradient potential, consisting of L sites, which is represented as follows,

$$\hat{H} = \sum_{j=1}^L \left[-t(e^{-g}\hat{b}_{j+1}^\dagger \hat{b}_j + e^g \hat{b}_j^\dagger \hat{b}_{j+1}) + U\hat{n}_j \hat{n}_{j+1} + \Delta_j \hat{n}_j \right]. \quad (1)$$

Here, L is the length of the lattice. t is the resonance amplitude, g is the non-Hermitian strength, U is the strength of the nearest-neighbor interaction. Δ_j represents the Stark gradient potential, which is defined as $\Delta_j \equiv -\gamma j + \alpha(j/L)^2$, where γ denotes the strength of the Stark gradient potential and α represents the curvature of the tail. The operators \hat{b}_j and \hat{b}_j^\dagger correspond to the annihilation and creation of spinless at site j , respectively. They obey the commutation relation $[\hat{b}_k, \hat{b}_l^\dagger] = \delta_{kl}$, and the particle number operator is denoted as $n_j \equiv \hat{b}_j^\dagger \hat{b}_j$.

A. Non-Hermitian level-spacing statistics

Firstly, we scrutinize the level-spacing distributions of non-Hermitian MBL systems. Level-spacing statistics effectively probe quantum system energy spectra, revealing Hamiltonian traits like integrable-chaotic spectra, quantum phase shifts, and symmetry-breaking phenomena. Nevertheless, owing to disparities in Hermitian characteristics, level-spacing statistical analysis employed in Hermitian systems cannot be directly utilized for non-Hermitian systems [57–59]. As a consequence of alterations in matrix symmetries, within the domain of non-Hermitian systems, the 10-fold Hermitian symme-

try classification expands to a 38-fold classification [60–62]. Since the eigenvalues in non-Hermitian systems are points distributed across a two-dimensional (2D) complex plane, complex level-spacing s_m serves as the statistical data. The geometric distance between the closest eigenvalues in the complex plane, denoted as s_α , is defined with $s_m \equiv \min_l |E_m - E_l|$ (unfolding) [43, 63].

As previously mentioned, for the delocalization phase, the non-Hermitian probability distribution $p(s)$ adheres to the Ginibre distribution $P_{Gin}^C(s) = cp(cs)$, which characterizes an ensemble of non-Hermitian Gaussian random matrices [59], with the specific form as follows:

$$p(s) = \lim_{N \rightarrow \infty} \left[\prod_{n=1}^{N-1} e_n(s^2) e^{-s^2} \sum_{n=1}^{N-1} \frac{2s^{2n+1}}{n! e_n(s^2)} \right] \quad (2)$$

where,

$$e_n(x) = \sum_{m=0}^n \frac{x^m}{m!} \quad (3)$$

and

$$c = \int_0^\infty ds p(s) = 1.1429 \dots \quad (4)$$

For the MBL phase, with the eigenenergies being localized on the real axis during this stage, the level-spacing statistics follow a Poisson distribution [59], denoted as

$$P_{Po}^R(s) = e^{-s}. \quad (5)$$

B. Eigenenergies with nonzero imaginary part ratio

Eigenenergies with a nonzero imaginary part ratio serve as a robust probe for detecting real-complex transitions of eigenenergies throughout the entire energy spectrum [43]. It is defined across the whole spectrum as

$$f_{Im} = D_{Im}/D. \quad (6)$$

Here, D_{Im} signifies the number of eigenenergies possessing non-zero imaginary components. To eliminate potential inaccuracies stemming from numerical techniques, eigenenergies E_α are deemed to have non-zero imaginary parts when $Im(E) \geq C$ ($C = 10^{-13}$). Concurrently, D represents the total number of eigenenergies. The scenario wherein all eigenenergies are purely real corresponds to $f_{Im} = 0$, while the converse limit, with all eigenenergies being complex, transpires at $f_{Im} = 1$.

C. Topological invariants in interaction non-Hermitian system

In one-dimensional interacting non-Hermitian systems, the winding number, defined on the complex plane, functions as the effective topological invariant. Gauge transformations $\hat{b}_j \rightarrow e^{i\frac{\Phi}{L}j} \hat{b}_j$ and $\hat{b}_j^\dagger \rightarrow e^{-i\frac{\Phi}{L}j} \hat{b}_j^\dagger$ are introduced

alongside parameter Φ (commonly interpreted as magnetic flux) to transform the model Hamiltonian into an effective form,

$$H(\Phi) = \sum_{j=1}^L [-t(e^{-g}e^{-i\frac{\Phi}{L}j}\hat{b}_{j+1}^\dagger\hat{b}_j + e^g e^{i\frac{\Phi}{L}j}\hat{b}_j^\dagger\hat{b}_{j+1}) + U\hat{n}_j\hat{n}_{j+1} + \Delta_j\hat{n}_j]. \quad (7)$$

Based on this transformation, the winding number is defined, denoted as

$$\omega_\Phi = \int_0^{2\pi} \frac{d\Phi}{2\pi i} \partial_\Phi \{H(\Phi) - E_B\} \quad (8)$$

Note that E_B refers to a specified reference point rather than the ground state energy. Departing from the traditional bulk-edge correspondence found in Hermitian systems, ω_Φ is used to compute the count of complex eigenenergy trajectory encirclements around the reference point E_B as the phase Φ transitions from 0 to 2π . Here, $\det H(\Phi)/|\det H(0)|$ is employed to characterize the winding number around the reference point E_B [64]. As a result, the winding number ω_Φ does not directly pertain to topological edge states but can be harnessed to unveil topological phase transitions.

D. Stability of the eigenstates

A hallmark of localized eigenstates is their robustness in the face of local disturbances [65]. A hallmark of localized eigenstates is their robustness in the face of local disturbances [49]. In the context of non-Hermitian quantum many-body systems maintaining TRS, localization prompts the vanishing of imaginary components in eigenenergies. Therefore, it becomes crucial to introduce localized perturbations to scrutinize the eigenstate responses to such perturbations, serving as a means to identify MBL phase transitions in non-Hermitian systems. Within this framework, we establish the stability of eigenstates as follows:

$$\mathcal{G} = \ln \frac{|\langle \varepsilon_{a+1}^l | \hat{V}_{NH} | \varepsilon_a^r \rangle|}{|\varepsilon'_{a+1} - \varepsilon'_a|} \quad (9)$$

Here, $|\varepsilon_a^l\rangle$ and $|\varepsilon_a^r\rangle$ represent the left and right eigenvectors, respectively. The perturbation term is given by $\hat{V}_{NH} = \hat{b}_j^\dagger\hat{b}_{j+1}$. We obtain $\varepsilon'_a = \varepsilon_a + \langle \varepsilon_a^l | \hat{V}_{NH} | \varepsilon_a^r \rangle$, with $\text{Im}(\varepsilon'_a) \leq C$. And the set $\{\varepsilon'_a\}$ is also positive, sorted in ascending order. For the delocalization phase, $\partial G/\partial L > 0$ is valid [66, 67], whereas for the localization phase, $\partial G/\partial L < 0$ is observed [68].

E. Dynamics of the half-chain entanglement entropy and the real part of energy

The half-chain entanglement entropy $S(t)$, it is given by

$$S(t) = -\text{Tr}[\rho(t) \ln \rho(t)], \quad (10)$$

where $\rho(t)$ represents the reduced density matrix, including quantum continuously measurements with no quantum jump [47]. Explicitly,

$$\rho(t) = \frac{\text{Tr}_{L/2} [|\varepsilon^r(t)\rangle \langle \varepsilon^r(t)|]}{|\varepsilon^r(t)\rangle \langle \varepsilon^r(t)|}. \quad (11)$$

Under conditions of extreme disorder or intense Stark potentials, highly excited eigenenergies transition to purely real values, significantly transforming the system's dynamical properties. The pivotal metric reflecting this shift in the system's dynamical behavior is the dynamics of the real part of energy [43]

$$E^R(t) = \text{Re}[\langle \Psi(t) | \hat{H} | \Psi(t) \rangle]. \quad (12)$$

And,

$$|\Psi(t)\rangle = \frac{e^{-i\hat{H}t} |\Psi_0\rangle}{\|e^{-i\hat{H}t} |\Psi_0\rangle\|}. \quad (13)$$

III. RESULTS AND DISCUSSION

In the current section, we utilize the exact diagonalization (ED) approach with the aid of the QuSpin package [69] to numerically derive the solutions pertaining to Eq. (1). The parameters of model are chosen as follows: $t = 1$, $U = 2$, and $g = 0.5$. A fixed particle-number subspace with $M = L/2$ particles is considered, which corresponds to a half-filled system.

A. MBL phase transition

In the analysis of non-Hermitian level-spacing statistics, we focus on the eigenenergies situated at the center of the spectrum, incorporating real and imaginary components within a $\pm 10\%$ range as specified in Ref.[43]. As illustrated in FIG. 1. (a), the distribution adheres to the Ginibre distribution when the Stark gradient potential strength is set at $\gamma = 0.2$. However, upon increasing the Stark gradient potential strength to $\gamma = 4.0$, the distribution transitions to follow the Poisson distribution, as FIG. 1. (b). This observation suggests that the system experiences a MBL phase transition in response to changes in the Stark gradient potential strength.

Upon confirming the existence of an MBL phase transition in the system, we begin to calculate critical information. Firstly, we consider the traditional half-chain entanglement entropy, restricting our calculations to right

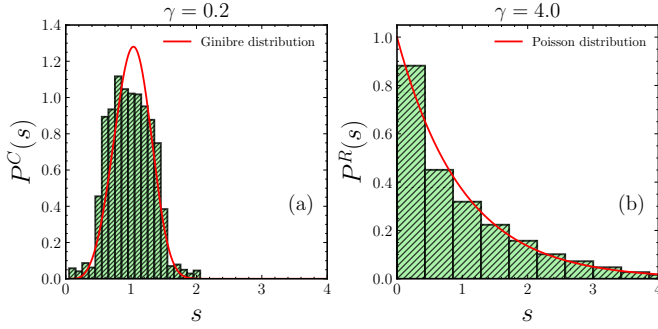


FIG. 1. Nearest-level-spacing distribution of (unfolded) eigenenergies on the complex plane for (a) $\gamma = 0.2$ with $L = 16$ and (b) $\gamma = 4.0$ with $L = 16$.

eigenstates $|\varepsilon_n^r\rangle$ within a central range of the real and imaginary parts, specifically those within $\pm 2\%$. The specific form is as follows: $S_n = \text{Tr}_{L/2} [|\varepsilon_n^r\rangle \langle \varepsilon_n^r|]$. FIG. 2. depicts the relationship between the selected eigenstate's half-chain entanglement entropy and the strength of the Stark gradient potential as a function of size L . In FIG. 2. (a), it is clearly visible that there is a transition from volume law to area law for the entanglement entropy around the critical point. We have set the function form for the critical scaling collapse as $(\gamma - \gamma_c)L^{1/\nu}$. FIG. 2. (b) presents the rescaled curve, from which we have identified the range of the critical point as $\gamma_c = 1.84 \pm 0.22$, and the critical exponent as $\nu = 0.90 \pm 0.10$. This situation bears similarities to that of Hermitian systems.

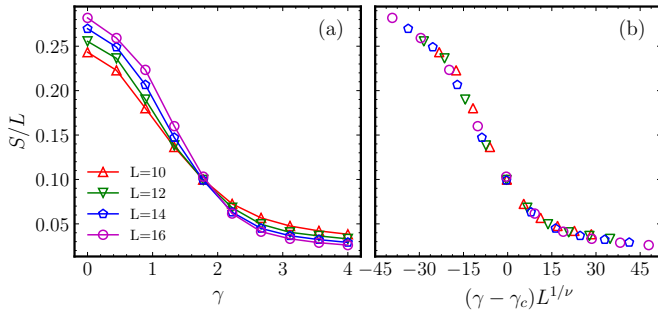


FIG. 2. In (a), the entanglement entropy per site, S/L , in the middle of the spectrum (considering eigenstates within a $\pm 2\%$ range around the real part of the eigenenergy spectrum) of the half-filled chain is examined. For smaller values of γ , S/L remains essentially constant, while for larger values of γ , it decreases as the system size L increases. In (b), we observe the collapse of critical scaling, with $\gamma_c = 1.84 \pm 0.22$ and $\nu = 0.90 \pm 0.1$.

However, for a non-Hermitian matrix, the choice of eigenstates can affect the quantitative results of the critical values. Therefore, we employ the stability of the eigenstate as a probe for the MBL. For the selection of local disturbance \hat{V}_{NH} , we adopt the same form as in Ref. [43]. As illustrated in FIG. 3., the results demonstrate the dependence of the stability of eigenstate \mathcal{G} on γ . Similar

to entanglement entropy, before the critical point γ_c , \mathcal{G} increases with the increase of size L , indicating a delocalization phase as represented by $\mathcal{G} \sim \zeta L$. After the critical point γ_c , \mathcal{G} decreases as size L grows, signifying a localization phase as represented by $\mathcal{G} \sim -\eta L$. We have pinpointed the critical value at $\gamma_c = 2.17 \pm 0.10$.

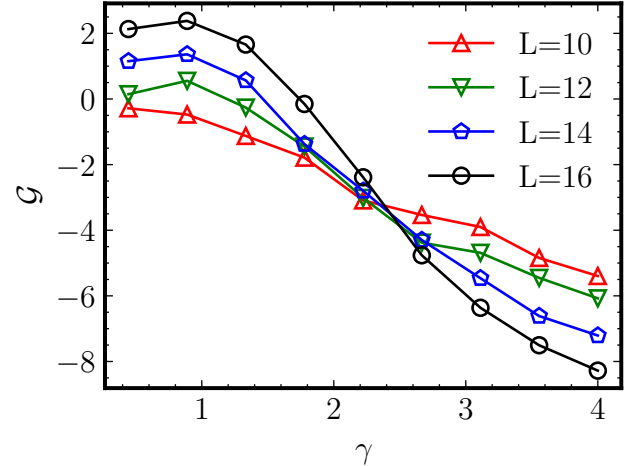


FIG. 3. Stability of eigenstates \mathcal{G} with real eigenenergies is examined as the Stark gradient potential strength γ is perturbed by the operator $\hat{V} = \hat{b}^\dagger j \hat{b} j + 1$. As γ increases, \mathcal{G} transitions from being approximately ζL to approximately $-\eta L$, where ζ and η are positive constants. This phase transition occurs at $\gamma_c = 2.17 \pm 0.10$.

B. Real-complex transition

Next, we examine the real-complex transition of the system's eigenvalues. We have plotted the eigenvalues at size $L = 12$ under $\gamma = 0.2$ and $\gamma = 4.0$, as shown in FIG. 4. (a) and (b) respectively. Since the system's TRS still holds, all eigenvalues with imaginary parts are symmetrically distributed along the real axis. It can be seen that when $\gamma = 0.2$, there are more eigenvalues with non-zero imaginary parts. However, when in a deeper MBL region, i.e., $\gamma = 4.0$, all eigenvalues fall on the real axis. This behavior mirrors that exhibited by disorder-driven non-Hermitian MBL systems.

FIG. 5. shows the relationship between the ratio of eigenenergies with nonzero imaginary part and γ . As depicted in FIG. 5. (a), before the critical point $\gamma_c^f = 0.42 \pm 0.10$, the value of f_{Im} increases with the growth of γ . After the critical point $\gamma_c^f = 0.42 \pm 0.10$, the value of f_{Im} decreases as γ increases. In FIG. 5. (b), we use the rescale function $(\gamma - \gamma_c)L^{1/\nu}$ to obtain a critical exponent of $\nu = 0.78 \pm 0.08$. This marks a significant divergence from disorder-driven non-Hermitian MBL systems. We speculate that under the thermodynamic limit $L \sim \infty$, γ_c and γ_c^f belong to different points. This fundamental difference stems from the distinct universal classes of critical properties induced by disorder-driven MBL phase tran-

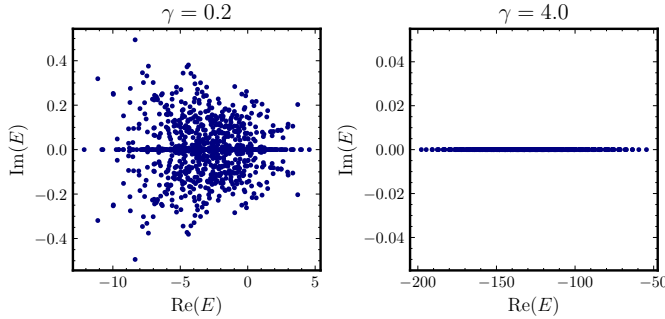


FIG. 4. The eigenenergies of the Hamiltonian, Eq.(1), are evaluated. Here, the lattice size is $L = 12$, non-Hermitian strength $g = 0.1$, and interaction strength $U = 1.0$. We consider two cases: (a) $\gamma = 0.2$ and (b) $\gamma = 4.0$.

sitions and Stark gradient potential-driven MBL phase transitions.

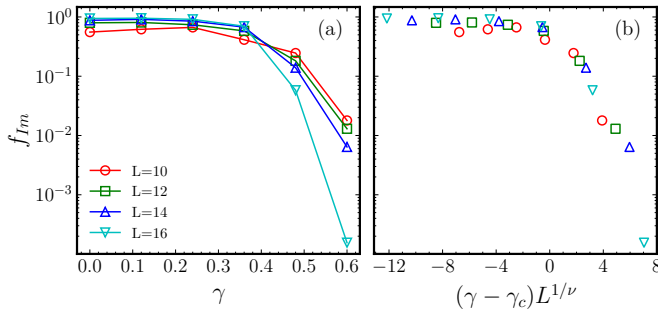


FIG. 5. In the model described by Eq.(1) with half-filling ($L=2M$), we examine the dependence of f_{Im} on γ . In this case, a real-complex transition occurs. The transition point is $\gamma_c^f = 0.42 \pm 0.10$.

C. Dynamics feature

We turn our attention to the system's dynamical response to phase transitions. As depicted in FIG. 6. (a), we observe the dynamic trajectory of the half-chain entanglement entropy in the Hermitian boundary case $g = 0$ and the non-Hermitian scenario $g = 0.1$. This is done for two distinct phases: a delocalization phase where $\gamma = 0.2 < \gamma_c$, and a localization phase where $\gamma = 4.0 > \gamma_c$. In FIG. 6. (a), when in the delocalization phase, there is a noticeable distinction between the Hermitian case (represented by the blue dashed line) and the non-Hermitian case (represented by the red solid line). In the Hermitian case, the entanglement entropy $S(t)$ initially increases, then stabilizes at around $S(t) \approx 3.4$. However, in the non-Hermitian case, it first increases, then decreases, and finally reaches a stable value. In contrast, when in the localization phase, both the Hermitian and non-Hermitian cases exhibit slow and consistent growth of $S(t)$. This result aligns with the dynamics of

entanglement entropy in disorder-driven MBL systems. We speculate that the difference in behavior between the Hermitian and non-Hermitian cases in the delocalization phase arises from the eigenstates of complex eigenvalues. However, in the localization phase, both the Hermitian and non-Hermitian cases exhibit consistent behavior due to the absence of eigenstates with non-zero imaginary parts. FIG. 6. (b) illustrates the response of the real part of the eigenenergy, denoted as $E^R(t)$, to the phase transition. It can be observed that for $\gamma \leq \gamma_c^f$, there is a slight decrease in $E^R(t)$ around $t = 10$ followed by stabilization. However, for $\gamma > \gamma_c^f$, this behavior is not observed. Overall, the response of $E^R(t)$ under the Stark gradient potential is not as pronounced as the response observed in disorder-driven systems.

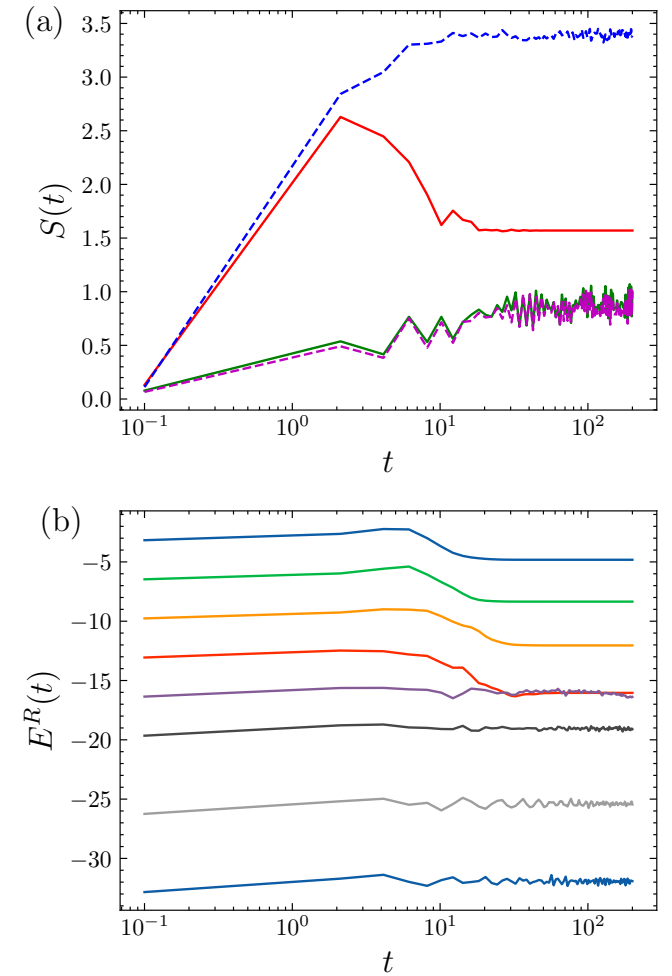


FIG. 6. The dynamics of the half-chain entanglement entropy $S(t)$ and the real part of the eigenenergies $E^R(t)$ are examined. (b), we show the time evolution of $S(t)$ for $g = 0.1$ (solid line) and $g = 0$ (dashed line). The lattice size is $L = 12$, and the initial state is $|\Psi\rangle_0 = |101010\cdots\rangle$. In addition, we present the time evolution of $E^R(t)$ for $g = 0.1$ and various values of γ : $\gamma = 0.1, 0.2, 0.3, 0.4, 0.5, 0.6, 0.8, 1.0$, and 1.2 (corresponding to the curves from top to bottom in (b)).

D. Phase diagram

Lastly, we have obtained phase diagrams for the non-Hermitian strength g and Stark gradient potential strength γ , as well as the interaction strength U and Stark gradient potential strength γ using the ED method, shown as FIG. 7. Our calculations consider cases with $L = 10, 12, 14, 16$.

In FIG. 7(a), we fixed the interaction strength $U = 1.0$, the blue dashed line on the left side corresponds to the increase of the eigenenergies with nonzero ratio f_{Im} as the size L increases, while the right side corresponds to the decrease of f_{Im} with increasing L . The black dotted line on the left side represents the increase of the stability of eigenstates \mathcal{G} with increasing size L , while the right side represents the decrease of \mathcal{G} as L increases. Region I denotes an area where both the stability of the eigenstates \mathcal{G} and the eigenenergies with nonzero ratio f_{Im} increase with the growth of dimension L . Region II represents an area where the stability of the eigenstates \mathcal{G} decreases with the expansion of dimension L , while the eigenenergies with nonzero ratio f_{Im} increase. Region III corresponds to an area where both the stability of the eigenstates \mathcal{G} and the eigenenergies with nonzero ratio f_{Im} decrease as the dimension L enlarges.

In FIG. 7(b), with the non-Hermitian strength set at $g = 0.1$, we identify three regions. Region I is characterized by an increase in both the stability of the eigenstates \mathcal{G} and the eigenenergies with nonzero ratio f_{Im} as the size L expands. Conversely, Region II depicts a scenario where the stability of eigenstates \mathcal{G} diminishes with an enlarging L , while the eigenenergies with nonzero ratio f_{Im} continue to rise. Lastly, Region III signifies an area where the stability of the eigenstates \mathcal{G} and the eigenenergies with nonzero ratio f_{Im} both decrease in response to the growth of L . The error bars are deduced from the shifts at the transition points across various system sizes. In the non-interacting limit where $U = 0$, the transitions coincide, which is consistent with the conclusions of [70]. This also implies that the spectral transition behavior exhibited by the MBL phase transition is consistent with the real-complex transition. However, in the presence of interactions, these two transitions separate as U increases. This suggests that an intermediate state may arise as the Stark gradient potential strength γ intensifies. This phenomenon has previously surfaced in the context of Stark MBL within the Hermitian framework [71].

IV. CONCLUSIONS

We have explored the MBL phase transition and the real-to-complex spectral transition in the non-Hermitian Hatano-Nelson model endowed with a Stark gradient potential and preserving TRS. Using numerical approaches, our investigation unveils the coexistence of MBL phase transitions and real-to-complex transitions within this

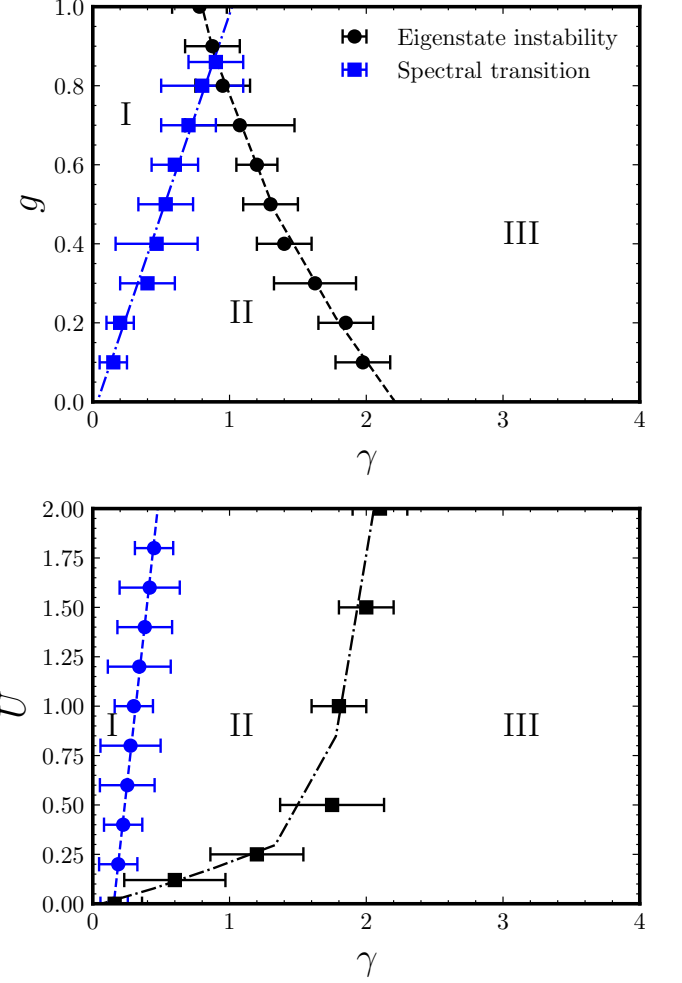


FIG. 7. The phase diagrams for the non-Hermitian strength g versus Stark gradient potential strength γ , and the interaction strength U versus Stark gradient potential strength γ are presented. In (a), for $t = 1.0$ and $U = 1.0$, the blue points represent the boundary of the complex eigenvalue ratio f_{Im} , and the black points represent the boundary of the stability of the eigenstates \mathcal{G} . The blue and black curves depict the fitting curves within the error range, dividing the entire region into three regions: I, II, and III. In (b), the case with a fixed $g = 0.1$ is considered.

model system. However, a marked distinction is observed when comparing these real-to-complex transitions to those found in disorder-driven non-Hermitian MBL systems. We propose that in the thermodynamic limit ($L \rightarrow \infty$), the critical points of these transitions will not align, a phenomenon attributable to Stark MBL and disorder-induced MBL (originating from random and quasiperiodic systems) being members of different universality classes at their critical junctures. Intriguingly, both disorder-driven MBL and Stark MBL systems display akin dynamical behaviors when it comes to entanglement entropy. Based on our phase diagram, a deeper exploration into the intermediate phase region of

non-Hermitian Stark MBL as an extension of Hermitian Stark MBL seems a natural progression. Further, probing the interconnections between non-Hermitian spectra and MBL avalanches promises to be a captivating avenue of investigation. We look forward to our findings being rapidly corroborated on ultra-cold atomic platforms.

ACKNOWLEDGMENTS

We gratefully acknowledge the National Natural Science Foundation of China (Grant No. 11874316), the

National Basic Research Program of China (Grant No. 2015CB921103), the Program for Changjiang Scholars and Innovative Research Team in University (Grant No. IRT13093), the Furong Scholar Program of Hunan Provincial Government (R.A.R.) for financial support, the Postgraduate Scientific Research Innovation Project of Hunan Province (Grant No. CX20210515), and the Xiangtan University.

[1] C. M. Bender, M. V. Berry, and A. Mandilara, Generalized \mathcal{PT} symmetry and real spectra, *Journal of Physics A: Mathematical and General* **35**, L467 (2002).

[2] W. D. Heiss, Exceptional points of non-hermitian operators, *Journal of Physics A: Mathematical and General* **37**, 2455 (2004).

[3] K. Ding, Z. Q. Zhang, and C. T. Chan, Coalescence of exceptional points and phase diagrams for one-dimensional \mathcal{PT} -symmetric photonic crystals, *Phys. Rev. B* **92**, 235310 (2015).

[4] Y. D. Chong, L. Ge, and A. D. Stone, \mathcal{PT} -symmetry breaking and laser-absorber modes in optical scattering systems, *Phys. Rev. Lett.* **106**, 093902 (2011).

[5] Z.-P. Liu, J. Zhang, i. m. c. K. Özdemir, B. Peng, H. Jing, X.-Y. Lü, C.-W. Li, L. Yang, F. Nori, and Y.-x. Liu, Metrology with \mathcal{PT} -symmetric cavities: Enhanced sensitivity near the \mathcal{PT} -phase transition, *Phys. Rev. Lett.* **117**, 110802 (2016).

[6] W. Chen, . Kaya zdemir, G. Zhao, J. Wiersig, and L. Yang, Exceptional points enhance sensing in an optical microcavity, *Nature* **548**, 192 (2017).

[7] C.-Y. Ju, A. Miranowicz, F. Minganti, C.-T. Chan, G.-Y. Chen, and F. Nori, Einstein's quantum elevator: Hermitization of non-hermitian hamiltonians via a generalized vielbein formalism, *Phys. Rev. Res.* **4**, 023070 (2022).

[8] S. Longhi, \mathcal{PT} -symmetric laser absorber, *Phys. Rev. A* **82**, 031801 (2010).

[9] N. Shukla, R. Modak, and B. P. Mandal, Uncertainty relation for non-hermitian systems, *Phys. Rev. A* **107**, 042201 (2023).

[10] A. S. Matsoukas-Roubeas, F. Roccati, J. Cornelius, Z. Xu, A. Chenu, and A. del Campo, Non-hermitian hamiltonian deformations in quantum mechanics, *Journal of High Energy Physics* **2023**, 60 (2023).

[11] R. Uzdin and N. Moiseyev, Scattering from a waveguide by cycling a non-hermitian degeneracy, *Phys. Rev. A* **85**, 031804 (2012).

[12] L. Feng, Z. J. Wong, R.-M. Ma, Y. Wang, and X. Zhang, Single-mode laser by parity-time symmetry breaking, *Science* **346**, 972 (2014).

[13] R. Lefebvre, O. Atabek, M. Šindelka, and N. Moiseyev, Resonance coalescence in molecular photodissociation, *Phys. Rev. Lett.* **103**, 123003 (2009).

[14] T. E. Lee, Anomalous edge state in a non-hermitian lattice, *Phys. Rev. Lett.* **116**, 133903 (2016).

[15] Z. H. Musslimani, K. G. Makris, R. El-Ganainy, and D. N. Christodoulides, Optical solitons in \mathcal{PT} periodic potentials, *Phys. Rev. Lett.* **100**, 030402 (2008).

[16] A. Guo, G. J. Salamo, D. Duchesne, R. Morandotti, M. Volatier-Ravat, V. Aimez, G. A. Siviloglou, and D. N. Christodoulides, Observation of \mathcal{PT} -symmetry breaking in complex optical potentials, *Phys. Rev. Lett.* **103**, 093902 (2009).

[17] A. A. Sukhorukov, Z. Xu, and Y. S. Kivshar, Nonlinear suppression of time reversals in \mathcal{PT} -symmetric optical couplers, *Phys. Rev. A* **82**, 043818 (2010).

[18] Q.-B. Zeng and R. L, Real spectra, anderson localization, and topological phases in one-dimensional quasireciprocal systems, *New Journal of Physics* **24**, 043023 (2022).

[19] A. Tuniz, T. Wieduwilt, and M. A. Schmidt, Tuning the effective \mathcal{PT} phase of plasmonic eigenmodes, *Phys. Rev. Lett.* **123**, 213903 (2019).

[20] V. Gurarie, Single-particle green's functions and interacting topological insulators, *Phys. Rev. B* **83**, 085426 (2011).

[21] A. Volya and V. Zelevinsky, Continuum shell model, *Phys. Rev. C* **74**, 064314 (2006).

[22] A. Volya and V. Zelevinsky, Discrete and continuum spectra in the unified shell model approach, *Phys. Rev. Lett.* **94**, 052501 (2005).

[23] P. Cejnar, S. Heinze, and M. Macek, Coulomb analogy for non-hermitian degeneracies near quantum phase transitions, *Phys. Rev. Lett.* **99**, 100601 (2007).

[24] Z. Gong, S. Higashikawa, and M. Ueda, Zeno hall effect, *Phys. Rev. Lett.* **118**, 200401 (2017).

[25] J. Alexandre, J. Ellis, and P. Millington, \mathcal{PT} -symmetric non-hermitian quantum field theories with supersymmetry, *Phys. Rev. D* **101**, 085015 (2020).

[26] M. Nakagawa, N. Kawakami, and M. Ueda, Non-hermitian kondo effect in ultracold alkaline-earth atoms, *Phys. Rev. Lett.* **121**, 203001 (2018).

[27] Z.-X. Guo, X.-J. Yu, X.-D. Hu, and Z. Li, Emergent phase transitions in a cluster ising model with dissipation, *Phys. Rev. A* **105**, 053311 (2022).

[28] J. A. S. Lourenço, R. L. Eneias, and R. G. Pereira, Kondo effect in a \mathcal{PT} -symmetric non-hermitian hamiltonian, *Phys. Rev. B* **98**, 085126 (2018).

[29] P. Barmettler and C. Kollath, Controllable manipulation and detection of local densities and bipartite entanglement in a quantum gas by a dissipative defect, *Phys. Rev. A* **84**, 041606 (2011).

[30] T. Fukuhara, S. Hild, J. Zeiher, P. Schauß, I. Bloch, M. Endres, and C. Gross, Spatially resolved detection of a spin-entanglement wave in a bose-hubbard chain, *Phys. Rev. Lett.* **115**, 035302 (2015).

[31] Y. Ashida, T. Shi, M. C. Bañuls, J. I. Cirac, and E. Demler, Solving quantum impurity problems in and out of equilibrium with the variational approach, *Phys. Rev. Lett.* **121**, 026805 (2018).

[32] M. Heyl, A. Polkovnikov, and S. Kehrein, Dynamical quantum phase transitions in the transverse-field ising model, *Phys. Rev. Lett.* **110**, 135704 (2013).

[33] N. Hatano and D. R. Nelson, Non-hermitian delocalization and eigenfunctions, *Phys. Rev. B* **58**, 8384 (1998).

[34] V. V. Konotop, J. Yang, and D. A. Zezyulin, Nonlinear waves in \mathcal{PT} -symmetric systems, *Rev. Mod. Phys.* **88**, 035002 (2016).

[35] S. Yao, F. Song, and Z. Wang, Non-hermitian chern bands, *Phys. Rev. Lett.* **121**, 136802 (2018).

[36] W. Chen, S. Cheng, J. Lin, R. Asgari, and G. Xianlong, Breakdown of the correspondence between the real-complex and delocalization-localization transitions in non-hermitian quasicrystals, *Phys. Rev. B* **106**, 144208 (2022).

[37] N. Hatano, Localization in non-hermitian quantum mechanics and flux-line pinning in superconductors, *Physica A: Statistical Mechanics and its Applications* **254**, 317 (1998).

[38] S. Weidemann, M. Kremer, S. Longhi, and A. Szameit, Topological triple phase transition in non-hermitian floquet quasicrystals, *Nature* **601**, 354 (2022).

[39] W. Wang, X. Wang, and G. Ma, Non-hermitian morphing of topological modes, *Nature* **608**, 50 (2022).

[40] Q. Liang, D. Xie, Z. Dong, H. Li, H. Li, B. Gadway, W. Yi, and B. Yan, Dynamic signatures of non-hermitian skin effect and topology in ultracold atoms, *Phys. Rev. Lett.* **129**, 070401 (2022).

[41] K. Zhang, Z. Yang, and C. Fang, Universal non-hermitian skin effect in two and higher dimensions, *Nature Communications* **13**, 2496 (2022).

[42] S. Longhi, Topological phase transition in non-hermitian quasicrystals, *Phys. Rev. Lett.* **122**, 237601 (2019).

[43] R. Hamazaki, K. Kawabata, and M. Ueda, Non-hermitian many-body localization, *Phys. Rev. Lett.* **123**, 090603 (2019).

[44] L.-J. Zhai, S. Yin, and G.-Y. Huang, Many-body localization in a non-hermitian quasiperiodic system, *Phys. Rev. B* **102**, 064206 (2020).

[45] L.-Z. Tang, G.-Q. Zhang, L.-F. Zhang, and D.-W. Zhang, Localization and topological transitions in non-hermitian quasiperiodic lattices, *Phys. Rev. A* **103**, 033325 (2021).

[46] Z. Xiao, K. Kawabata, X. Luo, T. Ohtsuki, and R. Shindou, Level statistics of real eigenvalues in non-hermitian systems, *Phys. Rev. Res.* **4**, 043196 (2022).

[47] V. Khemani, S. P. Lim, D. N. Sheng, and D. A. Huse, Critical properties of the many-body localization transition, *Phys. Rev. X* **7**, 021013 (2017).

[48] V. Khemani, D. N. Sheng, and D. A. Huse, Two universality classes for the many-body localization transition, *Phys. Rev. Lett.* **119**, 075702 (2017).

[49] A. Smith, J. Knolle, D. L. Kovrizhin, and R. Moessner, Disorder-free localization, *Phys. Rev. Lett.* **118**, 266601 (2017).

[50] H. Lang, P. Hauke, J. Knolle, F. Grusdt, and J. C. Halimeh, Disorder-free localization with stark gauge protection, *Phys. Rev. B* **106**, 174305 (2022).

[51] W. Morong, F. Liu, P. Becker, K. S. Collins, L. Feng, A. Kyprianidis, G. Pagano, T. You, A. V. Gorshkov, and C. Monroe, Observation of stark many-body localization without disorder, *Nature* **599**, 393 (2021).

[52] M. Schreiber, S. S. Hodgman, P. Bordia, H. P. Lschen, M. H. Fischer, R. Vosk, E. Altman, U. Schneider, and I. Bloch, Observation of many-body localization of interacting fermions in a quasirandom optical lattice, *Science* **349**, 842 (2015).

[53] M. Schulz, C. A. Hooley, R. Moessner, and F. Pollmann, Stark many-body localization, *Phys. Rev. Lett.* **122**, 040606 (2019).

[54] D. Emin and C. F. Hart, Existence of wannier-stark localization, *Phys. Rev. B* **36**, 7353 (1987).

[55] Y.-Y. Wang, Z.-H. Sun, and H. Fan, Stark many-body localization transitions in superconducting circuits, *Phys. Rev. B* **104**, 205122 (2021).

[56] J. Mk, M. J. Bhaseen, and A. Pal, Statics and dynamics of non-hermitian many-body localization (2023), arXiv:2301.01763 [cond-mat.dis-nn].

[57] A. M. García-García, L. Sá, and J. J. M. Verbaarschot, Symmetry classification and universality in non-hermitian many-body quantum chaos by the sachdev-ye-kitaev model, *Phys. Rev. X* **12**, 021040 (2022).

[58] O. Giraud, N. Macé, E. Vernier, and F. Alet, Probing symmetries of quantum many-body systems through gap ratio statistics, *Phys. Rev. X* **12**, 011006 (2022).

[59] F. Haake, Level repulsion, in *Quantum Signatures of Chaos* (Springer Berlin Heidelberg, Berlin, Heidelberg, 2010) pp. 47–59.

[60] K. Kawabata, K. Shiozaki, M. Ueda, and M. Sato, Symmetry and topology in non-hermitian physics, *Phys. Rev. X* **9**, 041015 (2019).

[61] A. Altland and M. R. Zirnbauer, Nonstandard symmetry classes in mesoscopic normal-superconducting hybrid structures, *Phys. Rev. B* **55**, 1142 (1997).

[62] H. Zhou and J. Y. Lee, Periodic table for topological bands with non-hermitian symmetries, *Phys. Rev. B* **99**, 235112 (2019).

[63] R. Hamazaki, K. Kawabata, N. Kura, and M. Ueda, Universality classes of non-hermitian random matrices, *Phys. Rev. Res.* **2**, 023286 (2020).

[64] M. Arikawa, I. Maruyama, and Y. Hatsugai, Topological quantum phase transition in the bec-bcs crossover, *Phys. Rev. B* **82**, 073105 (2010).

[65] M. Serbyn, Z. Papić, and D. A. Abanin, Criterion for many-body localization-delocalization phase transition, *Phys. Rev. X* **5**, 041047 (2015).

[66] W. Beugeling, R. Moessner, and M. Haque, Off-diagonal matrix elements of local operators in many-body quantum systems, *Phys. Rev. E* **91**, 012144 (2015).

[67] E. Khatami, G. Pupillo, M. Srednicki, and M. Rigol, Fluctuation-dissipation theorem in an isolated system of quantum dipolar bosons after a quench, *Phys. Rev. Lett.* **111**, 050403 (2013).

[68] J. Z. Imbrie, Diagonalization and many-body localization for a disordered quantum spin chain, *Phys. Rev. Lett.* **117**, 027201 (2016).

[69] P. Weinberg and M. Bukov, QuSpin: a Python package for dynamics and exact diagonalisation of quantum many body systems. Part II: bosons, fermions and higher spins, *SciPost Phys.* **7**, 020 (2019).

- [70] P. W. Brouwer, P. G. Silvestrov, and C. W. J. Beenakker, Theory of directed localization in one dimension, [Phys. Rev. B **56**, R4333 \(1997\)](#).
- [71] X. Wei, X. Gao, and W. Zhu, Static and dynamical stark many-body localization transition in a linear potential, [Phys. Rev. B **106**, 134207 \(2022\)](#).